Water-soluble polysaccharides promoting production of redispersible nanocellulose

Hu, Liqiu; Xu, Wenyang; Gustafsson, Jan; Koppolu, Rajesh; Wang, Qingbo; Rosqvist, Emil; Sundberg, Anna; Peltonen, Jouko; Willför, Stefan; Toivakka, Martti; Xu, Chunlin

Published in:
Carbohydrate Polymers

DOI:
10.1016/j.carbpol.2022.119976

Published: 01/12/2022

Document Version
Accepted author manuscript

Supplementary Information

Water-soluble polysaccharides promoting production of redispersible nanocellulose

Liqiu Hu [a], Wenyang Xu [a] *, Jan Gustafsson [a], Rajesh Koppolu [a], Qingbo Wang [a], Emil Rosqvist [b], Anna Sundberg [a], Jouko Peltonen [b], Stefan Willför [a], Martti Toivakka [a], Chunlin Xu [a] *

[a] *Laboratory of Natural Materials Technology, Åbo Akademi University, Henrikinkatu 2, Turku FI-20500, Finland;*

[b] *Laboratory of Molecular Science and Engineering, Åbo Akademi University, Henrikinkatu 2, Turku FI-20500, Finland;*

**Corresponding authors: wenyang.xu@abo.fi and cxu@abo.fi*

Characterization:

1. Molar mass analyses

The molar mass of cm-GGM, GGM, cat-GGM and xylan was determined using high performance size exclusion chromatography (HPSEC) equipped with a differential refractive index concentration detector (RI) and a multi angle light scattering detector (MALS) in aqueous eluent. In brief, samples in mass of 6-8 mg were dissolved in ca. 1.5 mL distilled water to achieve a clear solution, following by filtration through 0.2 μm Nylon syringe filter prior to measurement. The HPSEC/MALS/RI system was operated under the following conditions: 40 °C column temperature; flow rate of 0.5 mL min^{-1}; dn/dc of 0.15 mL/g, injection volume of 100 μL. Data obtained was evaluated by using ASTRA software, version 7.3.2.

2. Rheological behaviour of fibre dispersions

The viscosity was determined with an MCR rheometer (Anton Paar MCR 702 Multidrive) with concentric cylinder geometry (CC27/T200/SS). The shear viscosity of the raw and redispersed MFC and MFC/PS 5% suspensions (0.4 wt%) was monitored by increasing the shear rate from 0.1 to 1000 s-1 at constant temperature (25 ℃). Similarly, the viscosity of MFC/cm-GGM (1%,

5%, 10% and 20%) before and after redispersion at 1.3 wt% was also evaluated with the MCR. Meanwhile, the yield stress is a factor to evaluate the fibre-to-fibre interaction of nanocellulose suspension, which could be obtained through fitting with the Casson equation as following: $\sqrt{\tau} = \sqrt{\tau_y} + \sqrt{\eta\gamma}$ (Rao, 2014).

3. Fibre size distribution using dynamic light scattering and fibre image analyser

The hydrodynamic diameter of the nanocellulose was analysed by dynamic light scattering (DLS) using a Zetasizer (Malvern instruments Ltd, UK, model: Nano-ZS) with the model of nanocellulose (RI index: 1.47), and surface charge of nanocellulose samples were measured with the zeta potential. The obtained samples were diluted to 0.01 wt% following sonication for 5 min prior to DLS measurement. For each sample, triplicate measurements were conducted where each measurement consisted of 17 runs (10 s each). The hydrodynamic diameters were obtained by applying the previously developed methods as reported (Ford et al., 1985). The fibre dimension of suspensions, at 15 mg/L solid content, were analysed using the fibre image analyser (FS5, Valmet Automation Ltd, Finland). The obtained suspensions were evaluated by pre-set measurement methods (average length, fines ratio, and fibrillation) of the FS5 instrument that was expressed using the microfibrillated cellulose grades. The fines ratio is calculated by the fines as percentage of arithmetic distribution, the particles with width of 10 to 75 μm and length of 0 to 7.2 mm are included in the fines ratio. The fibrillation is the projection area of fibrils in relation to the projection area of the entire object, which is scaled into a percentage. The results were presented though average value by three parallel measurements.

4. Fibre morphological analyses using TEM, AFM, and SEM

The morphology changes of the suspensions with and without PS addition (MFC and MFC/PS) were studied with a JEM-1400 PLUS TEM microscope (JEOL Ltd., Japan) in bright-field mode with an accelerating voltage of 80 kV. Diluted sample (0.01 wt%) with 5 μL was deposited on

the copper grid to wait for 3 min at environmental temperature. The excess of suspension was removed with filter paper, and then stained with 2 wt% uranyl acetates for 1.5 min, prior to measurement.

The surface topography of the spin-coated and residual films was analysed with a Multimode 8 AFM from Bruker AXS Inc. (Madison, WI, USA). Images were taken in air with a J scanner in tapping mode using NSC15/AIBS silicon cantilevers from MikroMasch (tip diameter of 8 nm, resonance frequency 325 kHz, Tallinn, Estonia). A minimum of three images (10 μm*10 μm) were taken per sample, and scans were performed over several portions of the films. Other than a simple first order flattening, no image processing was carried out. In addition, the cross section of the films was monitored with a scanning electron microscope (SEM) (Q250 FESG, FEI).

5. Mechanical properties of films

The tensile strength of the cast films was tested using an Instron instrument (Model: 2527.102, Instron Corp., High Wycombe, England,) equipped with a load cell of 10 kN at room temperature under relative humidity of 40 %. The gauge length was 30 mm, and the strain rate was 1 mm/min. The thickness of the films was measured ten times per sample with a Lorenz Wetter paper thickness meter (L&M micrometre SE250, Sweden). The results for each sample were calculated using the average value based on at least five replicates according to ASTM D638 standard. The Young's moduli were calculated from the slope at the low strain using Origin software 2019b version. The density of the films was calculated from a representative specimen of 3 ± 0.8 cm^2 in surface area and about 25 ± 1.6 μm in thickness by dividing the mass with the sample volume.

6. Film optical properties

The optical properties of transmittance rate and haze of the films was determined with a Shimadzu UV-2600 spectrometer (Kyoto, Japan) with an attached integrating sphere. The

74 transmittance rate of films was measured for the wavelength range 300–830 nm and the haze
75 was calculated according to the methods reported elsewhere (Chen et al., 2020; Zhu et al., 2013).
76
77
78

Table S1. Formulation of MFC mixed with polysaccharides

Samples	Mass ratio of MFC and PS (w/w)	Solid content of MFC suspension	Clogging? [a]	DS of polysaccharides	Molar mass of polysaccharides (kDa), Mw	Zeta potential (mv)	Density of suspension (tonne/m^3)	Energy consumption (kWh/tonne)
MFC	-[b]	0.4 %	No	-	-	0.17	0.92	7460
MFC/cm-GGM 5%	19:1	0.4 %	No	1.5	61		0.93	7458
MFC	-	1%	Yes	-	-			-
MFC/CMC 5%	19:1	1 %	No	0.87	160	-0.14		
MFC/CGG 5%	19:1	1 %	No	0.82	-	0.74		
MFC/Cat-GGM 5%	19:1	1 %	No	0.63	45	0.82		
MFC/cm-GGM 5%	19:1	1 %	No	1.5	61	-0.4	0.93	2984
MFC/GGM 5%	19:1	1 %	No	-	27	0.2		
MFC/Xylan 5%	19:1	1 %	No	-	51	0.1		
MFC		1.5 %	Yes	-	-			
MFC/cm-GGM 1%	99:1	1.5 %	No	1.5	61			
MFC/cm-GGM 5%	19:1	1.5 %	No	1.5	61		0.93	1989
MFC/cm-GGM 10%	9:1	1.5 %	No	1.5	61			
MFC/cm-GGM 20%	4:1	1.5 %	No	1.5	61			

[a]: in the processing of homogenization, [b:] not detected.

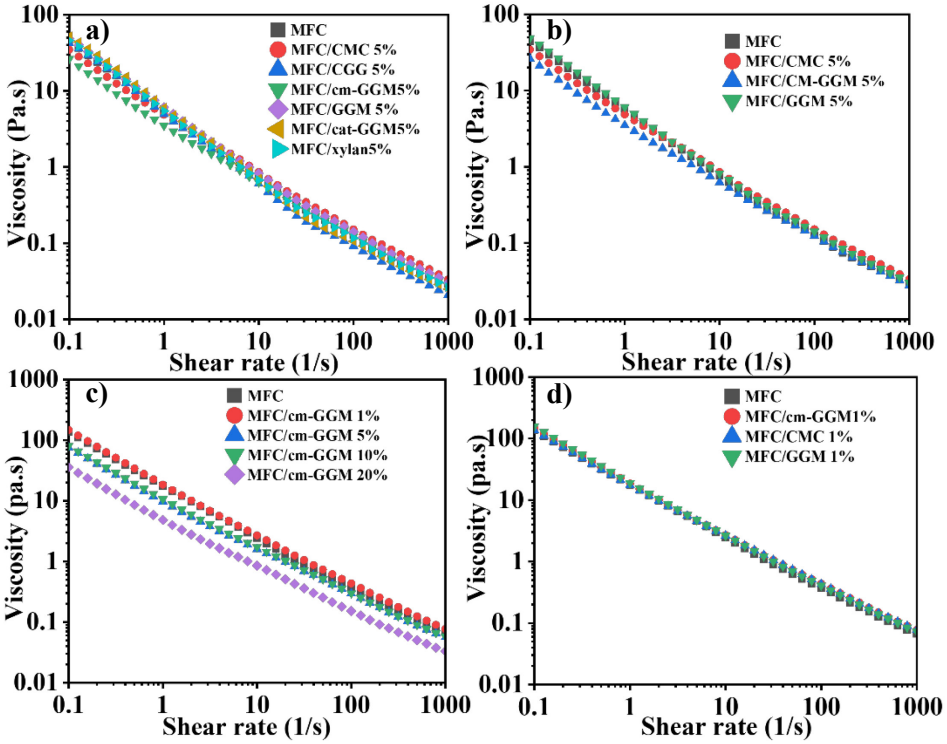

Figure S1. Viscosity profiles of MFC and MFC/PS blends before homogenization process. (a) MFC and MFC/ PS 5% at 1 wt% solid content), (b) MFC, MFC/CMC 5%, MFC/cm-GGM 5% and MFC/GGM 5% at 1 wt % solid content), (c) MFC and MFC/cm-GGM (1%-20%) at 1.5 wt.% solid content), (d) MFC, MFC/CMC 1%, MFC/cm-GGM 1% and MFC/GGM 1% at 1.5 wt%.

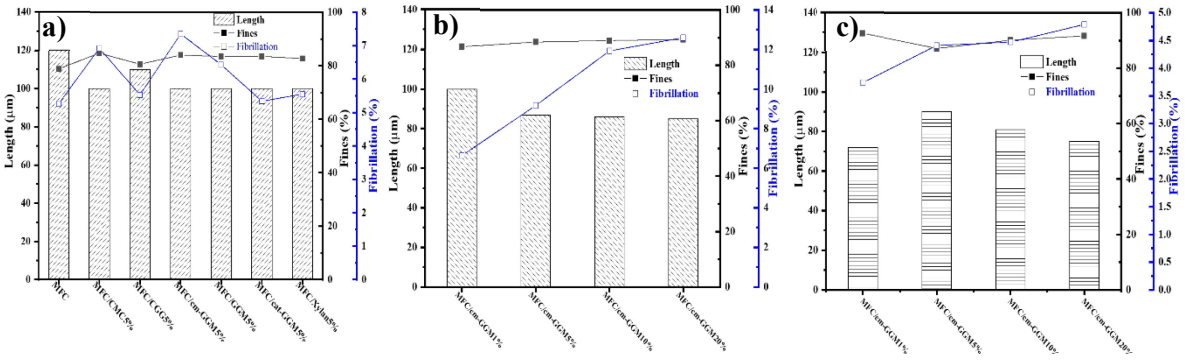

Figure S2. Fibre dimension of MFC and MFC/PS samples using FS5 image analyser. (a) MFC and MFC/PS 5% after redispersion; MFC/cm-GGM 1%, 5%, 10 % and 20% before(b) and after(c) redispersion, respectively.

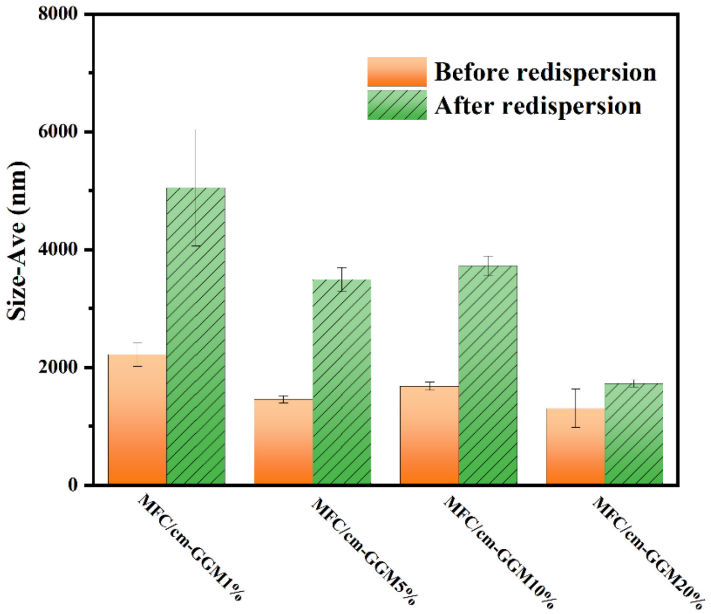

103

104 **Figure S3.** Size-average of and MFC/cm-GGM (1%-20%) before and after redispersion using DLS.

105

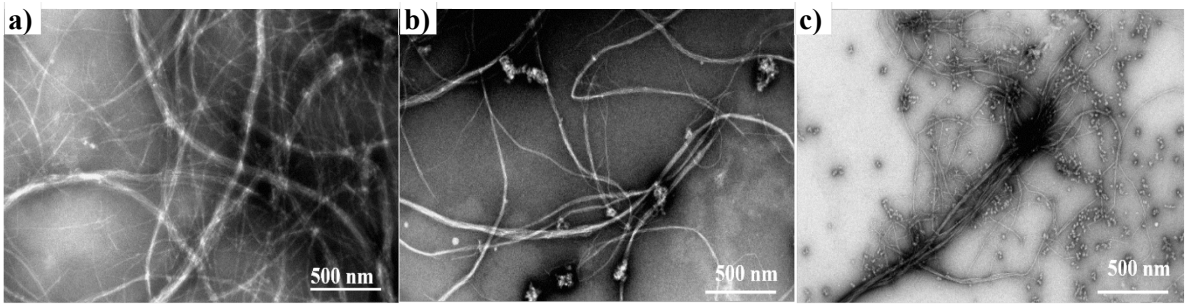

Figure S4. TEM images of MFC/PS 5% samples: (a) MFC/CGG 5%, (b) MFC/ cat-GGM 5%, and (c) MFC/xylan 5%.

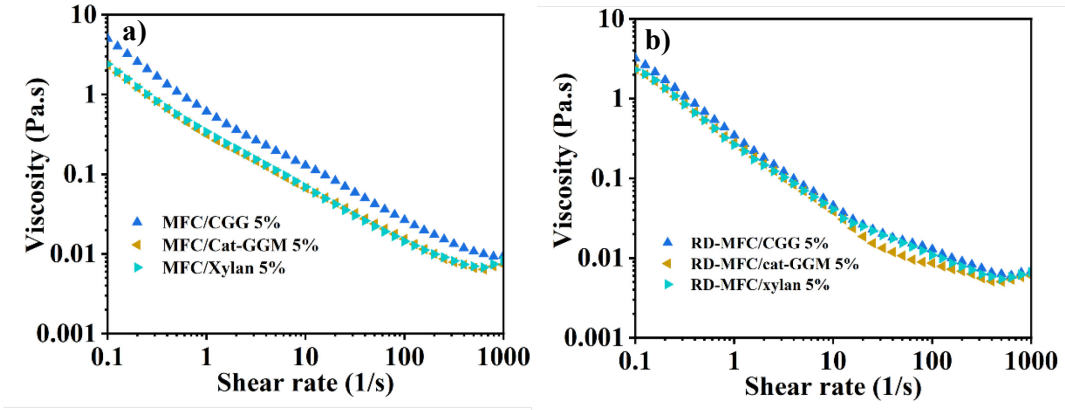

115

116 **Figure S5.** (a) Viscosity profile of MFC and MFC/PS 5% at 0.4 wt% solid content, (b) RD-MFC/PS 5% at 0.4

117 wt% solid content.

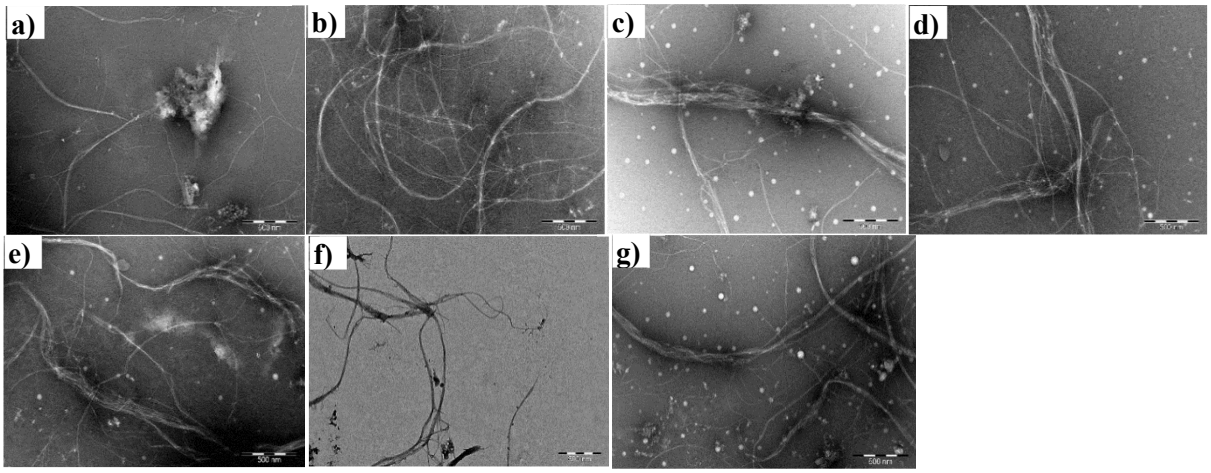

Figure S6. TEM images of MFC and MFC/PS 5% after redispersion: (a) RD-MFC, (b) RD-MFC/CMC 5%, (c) RD-MFC/CGG 5%, (d) RD-MFC/cm-GGM 5%, (e) RD-MFC/GGM 5%, (f) RD-MFC/ cat-GGM 5%, (g) RD-MFC/xylan 5%.

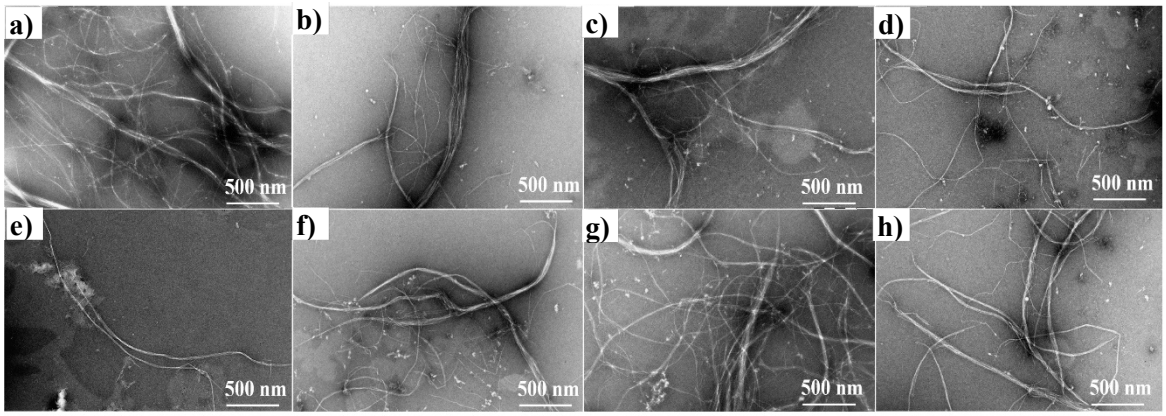

Figure S7. TEM images of MFC/cm-GGM samples before and after redispersion: (a) MFC/cm-GGM 1%, (b) MFC/cm-GGM 5%, (c) MFC/cm-GGM 10%, (d) MFC/cm-GGM 20%, (e) RD-MFC/cm-GGM 1%, (f) RD-MFC/cm-GGM 5%, (g) RD-MFC/cm-GGM 10%, and (h) RD-MFC/cm-GGM 20%.

Table S2. Physical properties of MFC and MFC/PS 5% samples before and after redispersion

Samples	Density (g/cm^3)	Tensile strength (MPa)	Young's modulus (GPa)	Strain at break (%)	Toughness (MJ/m^3)	Transmittance rate (%) at 550 nm	Haze (%) at 550 nm
MFC	1.32±0.06	61.98±4.9	7.3±0.6	1.4±0.2	34.7±12	74	83
MFC/CMC 5%	1.34±0.1	60.06±28.7	6.2±1.3	1.9±0.3	24.6±9	80	70
MFC/CGG 5%	1.26±0.05	78.72±10.4	5.8±0.4	1.8±0.5	74.9±10	60	93
MFC/cm-GGM 5%	1.31±0.06	116.56±25.6	6.3±0.4	3.1±0.4	153.8±8	77	68
MFC/GGM 5%	1.24±0.05	111.20±3.7	6.6±0.3	2.4±0.2	152.0±6	72	81
MFC/cat-GGM 5%	1.21±0.03	106.19±26.1	5.8±0.3	2.1±0.7	108.5±13	70	89
MFC/xylan 5%	1.32±0.04	104.27±6.8	6.3±0.4	1.8±0.1	99.5±10	68	81
RD-MFC	1.24±0.05	57.03±13.8	5.3±0.2	1.32±0.2	36.2±15	72	89
RD-MFC/CMC 5%	1.23±0.07	46.54±25.1	5.4±0.5	1.12±0.5	17.2±10	79	78
RD-MFC/CGG 5%	1.14±0.04	63.87±12.4	4.7±0.3	2.1±0.3	101.3±12	54	95
RD-MFC/cm-GGM 5%	1.10±0.04	112.1±14.1	5.2±0.2	3.87±0.6	188.1±8	74	82
RD-MFC/GGM 5%	1.09±0.02	94.19±10.4	5.2±0.3	2.65±0.5	145.4±9	59	93
RD-MFC/cat-GGM 5%	1.11±0.07	93.82±12.3	4.7±0.5	3.4±0.4	151.6±12	54	95
RD-MFC/xylan 5%	1.15±0.03	80.36±15.1	5.1±0.1	2.4±0.8	111.2±5	67	90

153 **Table S3.** Physical properties of MFC/cm-GGM (1%, 5%, 10% and 20%) films before and after redispersion

Samples	Density (g/cm^3)	Tensile strength (MPa)	Young´s modulus (GPa)	Strain at break (%)	Toughness (MJ/m^3)	Transmittance rate (%) at 550nm	Haze (%) at 550nm
MFC[a]	-	-	-	-	-	-	-
MFC/cm-GGM 1%	1.28±0.1	36.51±18.5	7.4±0.5	7±0.6	3.5±8	83	55
MFC/cm-GGM 5%	1.25±0.02	76.37±12.4	6.4±0.3	0.7±0.4	53.3±10	82	48
MFC/cm-GGM 10%	1.23±0.11	66.26±15.6	6.8±0.3	1±0.4	35.8±12	81	50
MFC/cm-GGM 20%	1.28±0.1	56.7±24.9	7.3±0.4	0.8±0.3	34.3±9	81	50
RD-MFC/cm-GGM 1%	0.77±0.2	26.27±7.4	3.3±0.4	1.2 ±0.4	5.4±7	74	84
RD-MFC/cm-GGM 5%	0.94±0.04	70.26±9.6	4.4±0.2	1.65±0.3	45.9±12	73	80
RD-MFC/cm-GGM 10%	0.98±0.02	59.5±5.1	4.9±0.3	1.35±0.3	36.5±10	80	72
RD-MFC/cm-GGM 20%	1.08±0.04	51.7±10.9	5.3±0.3	1.18±0.5	34.7±8	78	77

[a]: it´s not possible to obtain the MFC suspensions using homogenization under 1.5 wt% solid content suspensions

154
155
156
157
158
159

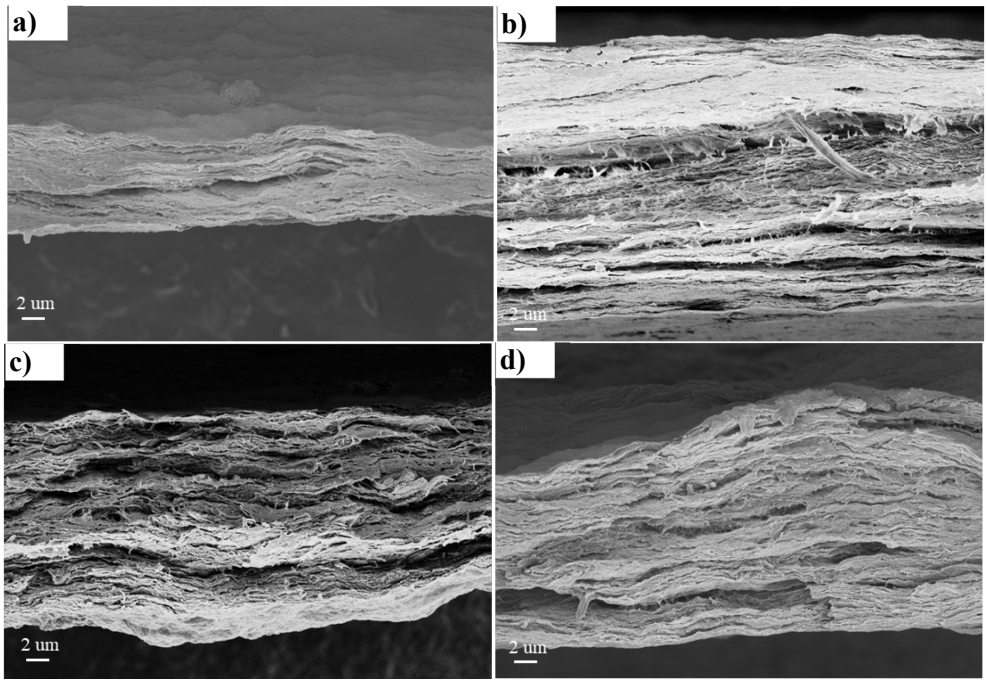

Figure S8. SEM cross section of films of MFC and MFC/cm-GGM 5%. Before redispersion: (a) MFC, (b) MFC/cm-GGM 5%, after redispersion: (c) RD-MFC, (d) RD-MFC/cm-GGM 5%.

Reference:

Rao, M. Rheological Behavior of Processed Fluid and Semisolid Foods. In: Rheology of Fluid, Semisolid, and Solid Foods. Food Engineering Series. Springer, Boston, MA. 2014, 231-329.

Ford, N. C. Light Scattering Apparatus. In Dynamic Light Scattering; Springer US, 1985; 7–58.

Chen, F.; Xiang, W.; Sawada, D.; Bai, L.; Hummel, M.; Sixta, H.; Budtova, T. Exploring Large Ductility in Cellulose Nanopaper Combining High Toughness and Strength. ACS Nano 2020, 14, 11150–11159.

Zhu, H.; Parvinian, S.; Preston, C.; Vaaland, O.; Ruan, Z.; Hu, L. Transparent Nanopaper with Tailored Optical Properties. Nanoscale, 2013, 5 (9), 3787–3792.